Macromolecules

ARTICLE

pubs.acs.org/Macromolecules

Characterization of Nanoporous Polystyrene Thin Films by Environmental Ellipsometric Porosimetry

Marylène Vayer,[†] Thi Hoa Nguyen,[†] David Grosso,[‡] Cédric Boissiere,[‡] Marc A. Hillmyer,[§] and Christophe Sinturel*[,†]

[†]Centre de Recherche sur la Matière Divisée, 1b rue de la Férollerie, 45 071 Orléans, France

[‡]Laboratoire Chimie de la Matière Condensée de Paris, UMR UPMC-CNRS 7574, Université Pierre et Marie Curie, Collège de France, 11 place Marcelin Berthelot, 75231 Paris, France

[§]Department of Chemistry, University of Minnesota, Minneapolis, Minnesota 55455-0431, United States

ABSTRACT:

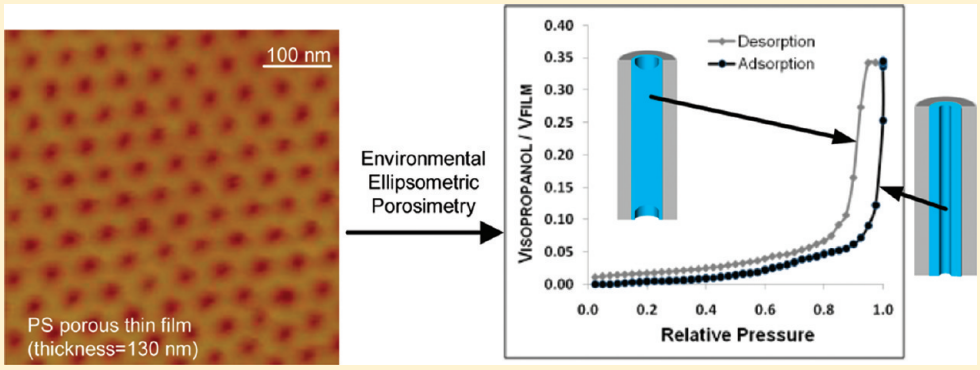

Environmental ellipsometric porosimetry (EEP) was used to characterize nanoporous polystyrene thin films containing cylindrical channels oriented perpendicularly to the surface of the film. These samples were prepared from the selective etching of polylactide from a self-assembled polystyrene−polylactide block copolymer. Isopropanol adsorption−desorption isotherms were obtained from the refractive index variations induced by the adsorption and condensation in the pores. Mean pore size and pore-size distributions were consistent with the values obtained by AFM, SEM, and GI-SAXS. More detailed analysis of the EEP data revealed that the topology of the porous structure was more tortuous than the simple picture of vertically oriented nanochannels might suggest. This was confirmed by preparing inorganic replicas that provided a hard negative copy of the porous network of the film. Microscopy on these replicas confirmed that a fraction of the channels exhibited a U-shape and thus were not perfectly perpendicular to the film surface.

INTRODUCTION

To move beyond the characteristic length limits imposed by conventional fabrication techniques of miniaturized devices, bottom-up technologies based on self-assembly of nanoscale building blocks have garnered a great deal of interest. Block copolymers are particularly promising candidate materials due to their natural tendency to form compositional heterogeneities on the nanometer length scale and organize in regular morphologies with tunable dimensions, shapes, and periodicity.[1] In the form of thin films, block copolymers can be applied in various nanotechnological processes, wherein the distinct microphase-separated domains[2] can be used for pattern transfer protocols.[3] Many diblock copolymers, with differential etch resistance toward selective degradation processes (e.g., chemical,[4] UV radiation,[5] plasma[6]), have been shown to be effective for providing nanoporous templates useful in, for example, high density storage array and integrated circuit element fabrication.[7]

One critical factor for success of this emerging technology is control of the topology of the pores within the film. This includes controlling connectivity, orientation, and accessibility to the interfaces (free surface and substrate). As block copolymer thin films are usually prepared by coating a polymer solution, the film is typically in a nonequilibrium state due the competition between phase separation kinetics and vitrification as the solvent evaporates; the microphase-separated domains display isotropic orientation with a high degree of connectivity.[8] As a result, electric field,[9] chemical patterned substrate,[10] thermal or solvent annealing,[11] or graphoepitaxy[12] approaches are typically required to achieve high degrees or order and structural fidelity. After selective etching of the minority component in the film, the structure of the nanoporous film is typically analyzed by imaging

Received: July 4, 2011
Revised: September 8, 2011
Published: October 24, 2011

the only free surface. Cross-sectional analysis allows the observation of the internal structure of the films, but this local information is not representative of the whole structure of the sample.

Environmental ellipsometric porosimetry (EEP) is now used in routine for the characterization of porosity in supported inorganic and hybrid nanoporous thin films. Initiated in the early 2000s by Balkanov and co-workers,[13] the ellipsometric porosimetry method is based on the measurement of the refractive index and thickness variations induced by the adsorption and condensation of solvent vapors in the pores of the sample being interrogated. Further developed for environmental analysis conditions, and called EEP,[14] this technique allows gas adsorption−desorption isotherms to be collected. These data can be used to determine the pore-size distribution and mechanical properties of films ranging from a few nanometers to micrometers thick. Because this method is simple, rapid, nondestructive, and reliable, EEP has become a popular analytical technique.[15] Nonetheless, EEP has never been used for the analysis of nanoporous polymer films. Application of EEP to nanoporous thin films from etchable block copolymer precursors ideally complements more traditional characterization techniques.

We utilize EEP to characterize the porous structure of polystyrene (PS) thin films, obtained from etching polylactide (PLA) from self-assembled coatings of polystyrene-*block*-polylactide (PS-*b*-PLA) block copolymers. The films were also characterized by conventional techniques including SEM, AFM, and GI-SAXS. The porosity characteristics obtained with these various investigation methods are compared and discussed. Specific information about the internal shape of the pores was obtained from EEP and confirmed by a detailed examination of an inorganic replica[16] of the porous polymeric supported layers.

EXPERIMENTAL SECTION

Preparation of the PS Porous Thin Films. Porous PS thin films with well-ordered cylindrical channels oriented perpendicularly to the surface of the film were prepared from self-assembled layer of PS-*b*-PLA following a procedure described elsewhere.[17] Briefly, the procedure includes the formation of thin films (100−150 nm) of PS-*b*-PLA by spin-coating, reorganization of the structure by solvent annealing, immobilization of the film on the substrate by UV irradiation, and then selective removal of the PLA domains by NaOH etching. Cylinder forming PS-*b*-PLA (90 kg mol^{-1}, PLA volume fraction $f_{PLA} = 0.34$) used for this study was obtained from the combination of anionic polymerization of styrene followed by the ring-opening polymerization of D,L-lactide.[18] Spin-coating solutions were prepared in chlorobenzene at a concentration of 20 mg mL^{-1} and deposited on Si substrates first at 300 rpm for 15 s and at 2000 rpm for 40 s. Solvent exposures were carried out in a closed 1.5 L desiccator at 20 °C with a reservoir of solvent (15 mL). UV irradiation to cross-link the PS phase was carried out in air at 365 nm (lamp power 40 W) for 1 h at a distance of 20 cm from the lamp. Hydrolysis of thin films was then performed by placing the sample in a 0.5 mol L^{-1} sodium hydroxide solution containing 40/60 (by volume) methanol/water for 30 min. After removing from the solution, the samples were washed with a 40/60 (by volume) methanol/water solution.

Preparation of Inorganic Replicas. Dense titania replica of the porous template was prepared by dip-coating the supported porous films from solutions having the molar composition: 1 $TiCl_4$, 5 H_2O, and 40 EtOH. Dip-coating was performed at room temperature, at ambient humidity, and at withdrawal speeds of 2 mm s^{-1}. The films were then heated at 450 °C for 5 min.

Characterization. Scanning electron microscopy (SEM) was carried out on a Hitachi S4200 device combined with an Oxford analyzer controlled by Link Isis software. An electron gun was equipped with a field emission electron source and was operated at 1 keV. SEM was performed in secondary electron mode. AFM in the tapping mode was carried out in air with a Nanoscope III from Digital Instruments Corp. The piezo scanner was able to scan with a horizontal range of 150 μm and a vertical range of 7 μm. Silicon cantilevers Tap 300 from Budget Sensors with integrated symmetrical pyramidal tips (15 μm high) with no Al coating backside, a nominal spring constant of 42 N m^{-1}, and a resonance frequency of 300 kHz were used.

EEP was carried with the experimental setup detailed in ref 14. Ellipsometric measurements were performed in the visible range (0.4−1.0 μm) at 70° incidence angle on a spectroscopic ellipsometer (Sopra) fitted with a cell allowing the environment control of the film. The partial pressure of the adsorbate in the cell was fixed using a controlled mixture of two air flows (via mass flow controllers), one of them being saturated in the adsorbate vapors. The temperature of the entire apparatus was set to 24 °C. Thicknesses and refractive indices were determined from the fits of the collected spectral data by using a classical Cauchy model. The three-layer model was used to describe the samples: (i) silicon substrate supporting a (ii) native silicon dioxide layer of 2 nm atop (iii) a layer being used for modeling the porous PS layer. From the analysis of the dry film assumed to be made of discrete domains of PS and voids, a Bruggeman effective medium approximation (BEMA) was used to determine the porous fraction f_{VOID}. In the BEMA model, the resulting optical properties (dielectric permittivity $\tilde{\varepsilon} = n^2$) of the film comprising PS and voids with known dielectric permittivities $\tilde{\varepsilon}_{PS}$ and $\tilde{\varepsilon}_{VOID}$ are then given by

$$f_{PS}\frac{\tilde{\varepsilon}_{PS} - \tilde{\varepsilon}}{\tilde{\varepsilon}_{PS} + 2\tilde{\varepsilon}} + f_{VOID}\frac{\tilde{\varepsilon}_{VOID} - \tilde{\varepsilon}}{\tilde{\varepsilon}_{VOID} + 2\tilde{\varepsilon}} = 0$$

where $f_{VOID} + f_{PS} = 1$.

From the variations of the refractive index as a function of the relative pressure of iPrOH (RP_{iPrOH}), classical adsorption−desorption curves $V_{iPrOH}/V_{film} = f(RP_{iPrOH})$ were extracted also using the BEMA model. For this purpose, we assume that for each value of RP_{iPrOH}, the optical properties of the film results from a combination of the optical properties of the dry film (material A, PS with empty pores at $RP_{iPrOH} = 0\%$) at a volume fraction f_A and the properties of the film with the pores completely filled by the solvent (material B, PS with isopropanol-filled pores at $RP_{iPrOH} = 100\%$) at a volume fraction f_B. This takes into account the variation of the optical properties of the solvent confined in the pores that would be needed if one had chosen to model the system as a mixture of the pure solvent and a porous PS matrix.[14] This computation approach takes into account the complex expression of the refractive index and is most accurate for a two-component system. In this BEMA model, the resulting optical properties (dielectric permittivity $\tilde{\varepsilon}$) of the film consisting of various volume fractions of the two materials A and B of known dielectric permittivity $\tilde{\varepsilon}_A$ and $\tilde{\varepsilon}_B$ is then given by

$$f_A\frac{\tilde{\varepsilon_A} - \tilde{\varepsilon}}{\tilde{\varepsilon_A} + 2\tilde{\varepsilon}} + f_B\frac{\tilde{\varepsilon_B} - \tilde{\varepsilon}}{\tilde{\varepsilon_B} + 2\tilde{\varepsilon}} = 0$$

Using this method, f_A and f_B as a function of the iPrOH content are then obtained by fitting the $n = f(RP_{iPrOH})$ curves. Using the measured value of f_{VOID} from analysis of the empty (i.e., dry) of $f_{VOID} = 0.34$, V_{iPrOH}/V_{film} is then given by $f_B \times f_{VOID}$.

Small-angle X-ray scattering in a grazing-incidence (GI-SAXS) was performed with a X-ray beam of photon energy 8.9 keV ($\lambda = 1.39$ Å) on the SWING beamline at SOLEIL synchrotron. The sample was placed at a distance of 1600 mm of the detector (CCD camera, AVIEX). The transmitted and specular reflected beams were masked by a vertical beam-stop.

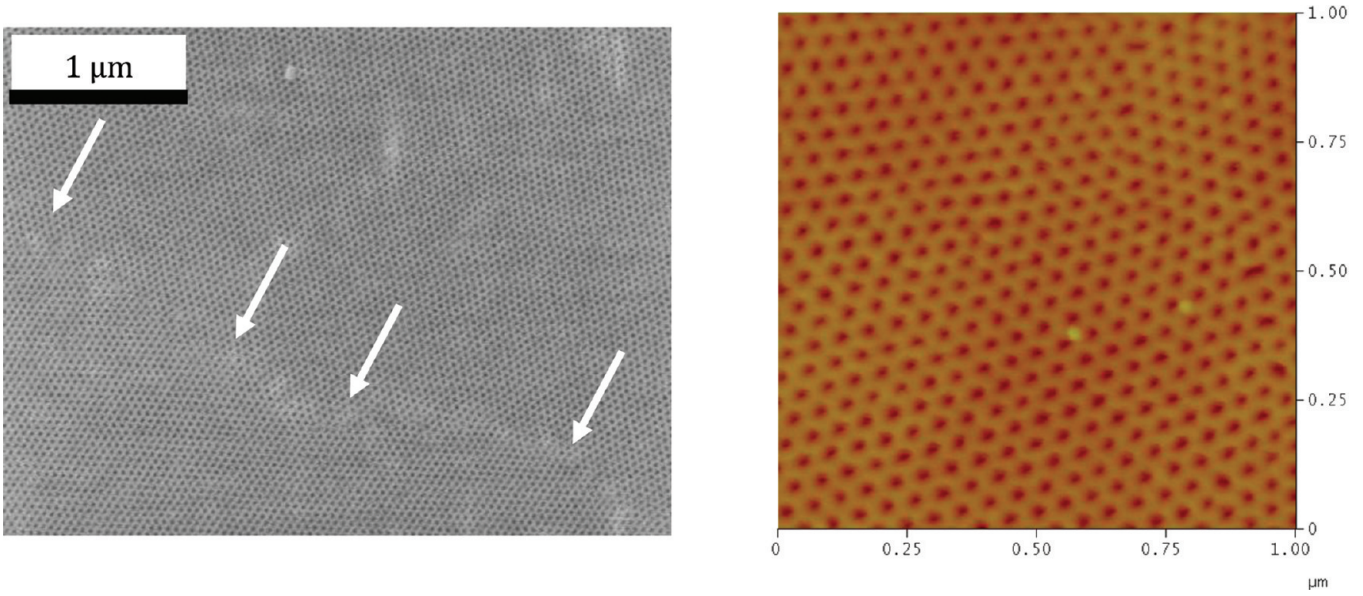

Figure 1. Top view SEM image of the block copolymer thins films after selective removal of the minor component (left). The arrows point out a grain boundary; 1 μm^2 AFM image showing grain boundary at the surface of the porous film (right).

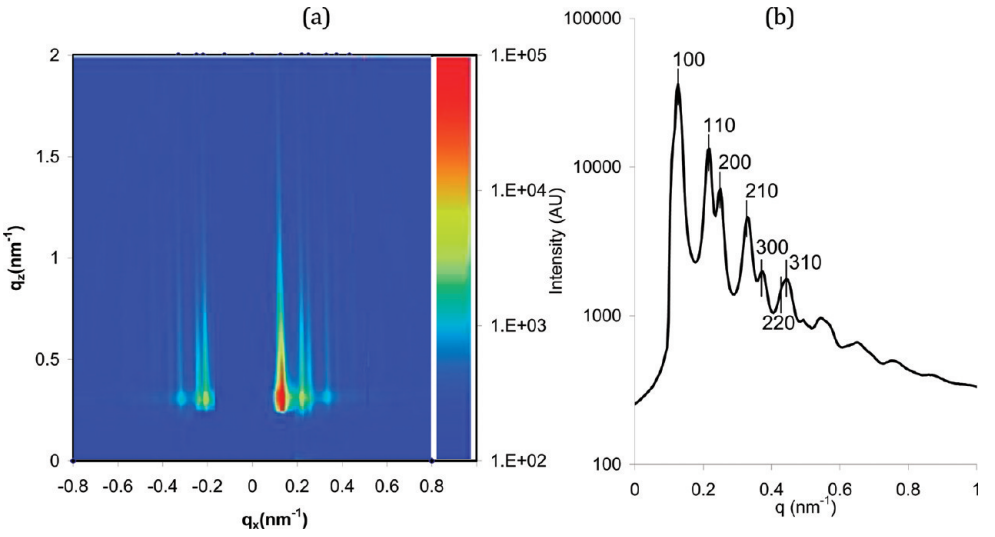

Figure 2. 2D GI-SAXS patterns of PS porous thin film (a); 1D profile (b).

RESULTS AND DISCUSSION

AFM, SEM, and GI-SAXS Characterization of the Nanoporous Thin Films. A typical SEM image of the nanoporous thin film is displayed in Figure 1. Channels resulting from the selective removal of the PLA emerge at the surface of the film and display the characteristic hexagonal structure consistent with the parent PS-*b*-PLA block copolymer morphology. Only a single grain boundary can be observed on this 20 μm^2 micrograph, consistent with a high degree of long-range order; a grain boundary is shown in more detail by AFM.

From a series of AFM images, we estimated a cylinder center-to-center distance of 57 ± 2 nm and a cylinder diameter of 28 ± 2 nm. This center-to-center distance was confirmed by synchrotron GI-SAXS measurements. Figure 2 displays the 2D GI-SAXS diffraction patterns of the porous PS films where multiple Bragg reflections were observed. The principal reflection is at q_0 = 0.125 nm^{-1}, and higher orders reflections are consistent with a hexagonal cylindrical arrangement of perpendicularly aligned cylinders with a center-to-center distance of 58 nm, consistent with the AFM images. From this center-to-center distance and the volume fraction of PLA in the starting block copolymer, the predicted cylinder diameter is 36 nm. The pore size determined by AFM is underestimated, and this was attributed the convolution of the tip with the sample topography which is known to introduce significant inaccuracy in an AFM image when the tip radius (estimated to be not less than 10 nm) is comparable to the typical dimension of the sample features to be observed.[19]

Environmental Ellipsometric Porosimetry. Figure 3 shows the variations of the refractive index and thickness measured by spectroscopic ellipsometry upon an adsorption−desorption cycle performed between 0 and 100% of the saturation vapor pressure

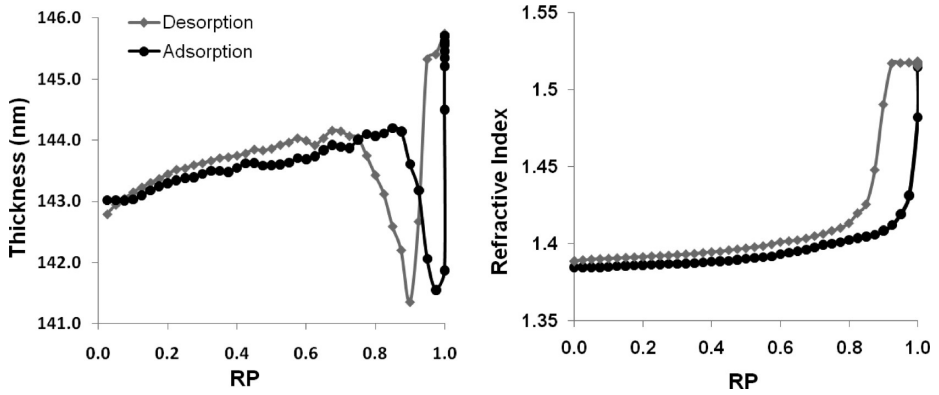

Figure 3. Thickness (left) and refractive index (right) isotherms of a supported porous PS film as a function of the relative pressure (RP) of iPrOH. T = 24 °C.

of isopropanol (iPrOH) (P^0_{iPrOH} = 41 mmHg at 24 °C). In dry air, the refractive index of the etched polymer layer is 1.39, which is lower than the value of the parent PS-*b*-PLA film (n_{700nm} = 1.56). This decrease of refractive index confirms the formation of voids in the materials due to PLA removal. The porous fraction f_{VOID} calculated from an ordinary Bruggeman effective medium approximation mixing optical properties of pure PS ($n_{PS,700nm}$ = 1.63) and voids (n = 1.00) is measured at 34%, which is in excellent agreement with the volume fraction of PLA into the copolymer.

In the case of porous polymer films, the difficulty for EEP analysis is the selection of an appropriate liquid to probe the porosity of the system. It must display favorable interactions with the pore walls but must not (significantly) swell the polymer matrix. In the case of inorganic systems, water is a common probe because of the hydrophilic nature of the walls and because virtually no diffusion occurs within the inorganic phase.[20] For this study, water, ethanol, isopropanol, THF, and acetone were tested for the EEP measurements. With water and EtOH, no significant swelling of the matrix was observed, but limited adsorption was obtained and no capillary condensation occurred at 100% of the saturated solvent vapor pressure. With THF and acetone, a large increase of the thickness was continuously monitored upon vapor solvent exposure, indicating unwanted swelling of the matrix. iPrOH displayed intermediate behavior, with no significant swelling of the PS matrix and sufficient adsorption into film pores. As observed in Figure 3, the variation of the refractive index upon iPrOH exposure displays typical hallmarks of such phenomenon with a slow increase up to a relative pressure (RP_{iPrOH}) of 0.8 due the adsorption of the vapors on the pore walls, followed by a sharp increase characteristic of the mesopores being filled due to capillary condensation of iPrOH. Only a 0.6% increase in thickness was observed up to RP_{iPrOH} = 0.8 consistent with very little swelling of the matrix during the experiment. For RP_{iPrOH} > 0.8 the thickness decrease is due to the appearance of a true liquid meniscus formed in the pores during the capillary condensation. The curvature of the meniscus generates a stress on the pore walls that increases as the pores are continuously filled. When the pores are completely filled, the curvature of the meniscus decreases and the stress is relaxed according to the Laplace law, leading to the final sharp thickness increase observed near P^0_{iPrOH}. All these phenomena have been well described in the case of inorganic and hybrid materials.[14]

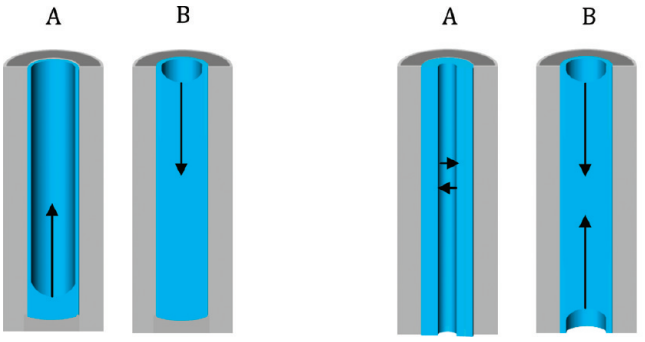

Figure 4. Schematic view of pores filling (A) and emptying (B) in a pore closed at one end (left) and in a pore open at both ends (right).

Hysteresis was observed during at high values of RP_{iPrOH} during desorption of the iPrOH. Nonetheless, the overall process is reversible as the final and initial states display similar values of thickness and refractive index. Such hysteresis can be due either to the presence of pore restrictions at the top of the film and/or to the isopropanol liquid meniscus geometry that is different for adsorption and desorption. From the AFM and SEM images in Figure 1, the pores are expected to be straight, monodisperse cylindrical channels with no restrictions. A perfect cylindrical pore closed at one end should exhibit capillary adsorption and desorption at similar RP (i.e., the liquid meniscus should present the same spherical geometry; see Figure 4). Thus, the presence of a hysteresis in this case could be explained by the existence of cylindrical pores that are open at both ends. This suggests that instead of being completely perpendicular, adjacent pores could be joined at the bottom of the film. This leads to a liquid meniscus presenting cylindrical geometry during the filling step and spherical geometry during the emptying step (Figure 4).

From the variations of the refractive index as a function of the pressure of iPrOH, classical adsorption−desorption curves $V_{iPrOH}/V_{film} = f(RP_{iPrOH})$ can be extracted using the BEMA model. This allows the calculation of the pore size distribution (PSD) from the adsorption curve (considering a cylindrical liquid meniscus) and from the desorption curve (considering a spherical liquid meniscus) using a modified Kelvin equation (Figure 5).[14] Both PSDs exhibit a large peak in the same pore size range. In spite of large errors due to the fact that capillary condensation occurs at very high RP (the precision of gas porosimetry

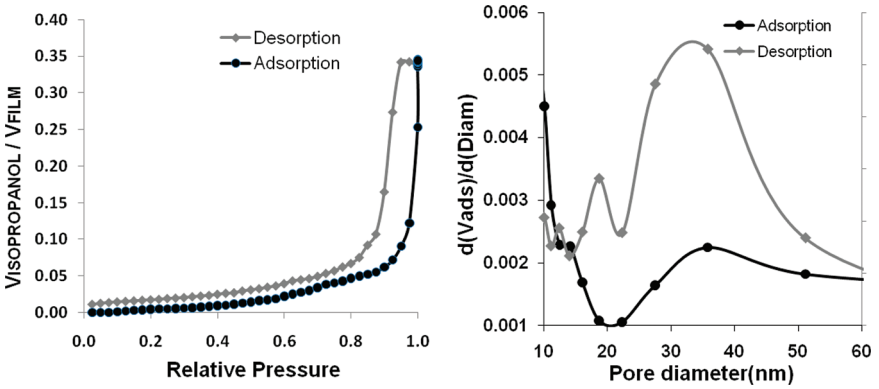

Figure 5. Adsorption−desorption isotherms (left) and pore size distributions (right) in a PS porous film obtained by considering a cylindrical liquid meniscus at the adsorption and a spherical liquid meniscus at the desorption.

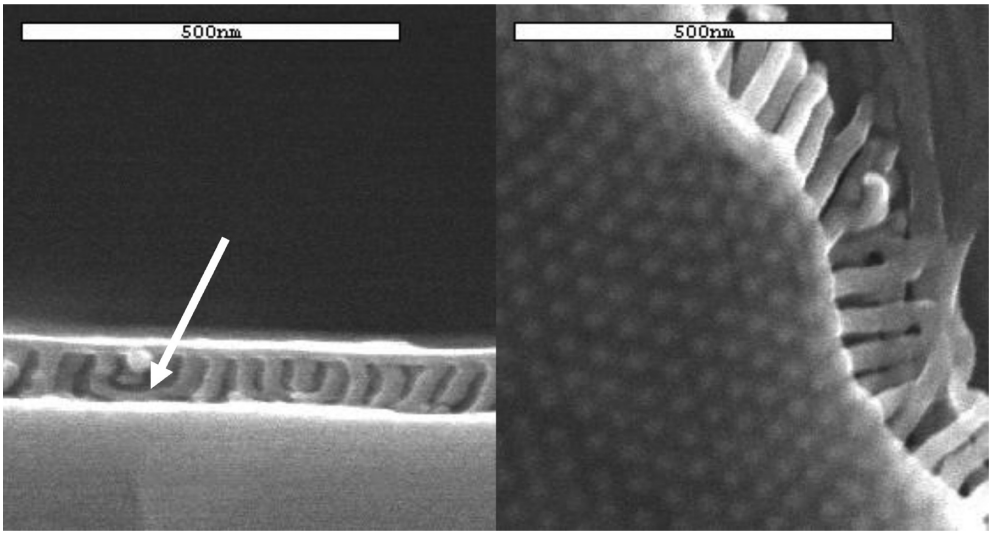

Figure 6. SEM side (left) and top (right) views of the TiO_2 replica of the porous PS film studied by EEP.

techniques decreases when the capillary condensation RP is close to saturation), both isotherm branches agree in estimating the pore size to be 31.5 ± 5 nm (estimated error based on experience). This is in reasonable agreement with the characteristic of the pore sizes extracted from GI-SAXS and AFM. There is a lower limit in pore size below the capillary condensation does not occur anymore and where the Kelvin equation is no longer valid. For water in ceramics, the limit is around 1 nm in diameter, although there is no broad agreement on this value as it also depends on the pore surface chemistry and morphology, the nature of the adsorbed molecules, etc.[21] In the present work, we are far from this critical limit as confirmed by the inorganic replication of the porous systems (see below). A spherical liquid meniscus during adsorption is unrealistic because it would have translated to a pore diameter larger than the *d*-spacing of the structure obtained by GI-SAXS (Figure 2). These data are consistent with pores of the PS film that are likely cylindrical with both ends opened, and it implies that a fraction of the pores must be interconnected. To confirm this hypothesis, the inorganic replication of the porous network has been performed to better understand the internal structure of the film.

Titania Replica. EEP analysis of these thin films suggests a complex pore topology and that the pores are actually not ideally perpendicular to the surface of the substrate for the film thickness interrogated. In parallel to EEP measurements, we developed an alternative method to investigate the internal structure of the film that consists of preparing the replica of the porous network by (i) filling the pores with a sol−gel solution containing titania precursors and (ii) thermal treatment at 500 °C that leads to PS decomposition and polycondensation of the sol−gel precursors.[16] This gives a hard replica of the porous network which is much easier to handle and characterize, providing complete information on the inner structure. This was applied to a representative porous PS sample studied by EEP in this study (i.e., the same thickness and solvent annealing time were used). Figure 6 displays the top and side view of the replica. The mode of preparation leads to simultaneous impregnation of the pores and a deposition of a top layer, leading to a final inorganic structure consisting in vertical nanopillars supporting a continuous roof. This can be clearly seen on the side view but also on the top view obtained in a crack. The side view reveals that a fraction of the pillars are connected along the interface with the substrate, leading to a characteristic U-shape (indicated by the arrow of the image). This indicates a defected pore structure and accounts for the desorption hysteresis observed in EEP. A significant fraction of the initial PLA domains displays a parallel orientation along the Si interface, although regular organization of the

PLA domains was observed from the top view of PS-*b*-PLA films.

CONCLUSION

Environmental ellipsometric porosimetry, restricted to the characterization of inorganic or hybrid supported layers, has been used to probe the internal porosity of nanoporous polystyrene thin films. Selecting a liquid that limits the swelling of the polystyrene, we showed that classical adsorption−desorption isotherms could be obtained from the refractive index variations of a porous polymer film in equilibrium with vapors of the liquid. In this work, the measurements were performed with iPrOH on a polystyrene film exhibiting a well-defined porosity obtained from the selective etching of a self-assembled film of polystyrene-*b*-polylactide block copolymer. In spite of errors due to the fact that capillary condensation occurs at very high RP_{iPrOH}, the calculation of the pore size distribution using a modified Kelvin equation in both isotherm branches (adsorption and desorption) led to a pore size consistent with that extracted from the microscopic study of the film (AFM) and the GI-SAXS measurements. Additional information concerning the topology of the porosity was obtained from the shape of the adsorption−desorption isotherms. The hysteresis suggests the existence of cylindrical pores opened at both ends, indicating that instead of being completely perpendicular with a circular base anchored at the surface of the substrate, some adjacent pores are connected at the substrate/film interface. This has been confirmed by examining a titania replica of the porous film where a fraction of the titania pillars were found to be connected along the interface with the substrate leading to a characteristic U-shape.

This method can be generalized to any type of porous polymer system, including those with more complex topology. The gyroid structure, which is particularly relevant for many practical applications, can be seen as an interconnected network of cylindrical pores that could be studied with the same mathematical treatment used for this system (Kelvin equation). For each porous sample, the crucial parameter will be the selection of an appropriate liquid to probe the porosity, dictated by the polymer/solvent interactions and the pore wall functionality. This latter point is now under careful investigation for porous PS systems bearing various degrees of hydrophilicity, where condensation of a more hydrophilic solvent (even water) should be possible.

AUTHOR INFORMATION

Corresponding Author

*E-mail: christophe.sinturel@univ-orleans.fr.

ACKNOWLEDGMENT

We acknowledge SOLEIL for provision of synchrotron radiation facilities, and we thank Olivier Lyon for assistance in using beamline SWING. M.A.H. thanks the National Science Foundation for support (DMR-1006370).

REFERENCES

(1) (a) Hamley, I. W. *The Physics of Block Copolymer*; Oxford University Press: New York, 1998. (b) Leibler, L. *Macromolecules* **1980**, *13*, 1602. (c) Matsen, M. W.; Bates, F. S. *Macromolecules* **1996**, *29*, 1091.

(2) Matsen, M. W. *Curr. Opin. Colloid Interface Sci.* **1998**, *3*, 40.

(3) (a) Park, C.; Yoon, J.; Thomas, E. L. *Polymer* **2003**, *44*, 6725. (b) Hamley, I. W. *Nanotechnology* **2003**, *14*, R39.

(4) Zalusky, A. S.; Olayo-Valles, R.; Wolf, J. H.; Hillmyer, M. A. *J. Am. Chem. Soc.* **2002**, *124*, 12761.

(5) Xu, X.; Kim, H.-C.; DeRouchey, J.; Seney, C.; Levesque, C.; Martin, P.; Stafford, C. M.; Russell, T. P. *Polymer* **2001**, *42*, 9091.

(6) Park, M.; Harrison, C.; Chaikin, P. M.; Register, R. A.; Adamson, D. H. *Science* **1997**, *276*, 1401.

(7) (a) Hong, A. J.; Liu, C. C.; Wang, Y.; Kim, J.; Xiu, F. X.; Ji, S. X.; Zou, J.; Nealey, P. F.; Wang, K. L. *Nano Lett.* **2010**, *10*, 224. (b) Stoykovich, M. P.; Kang, H.; Daoulas, K.Ch.; Liu, G.; Liu, C.-C.; de Pablo, J. J.; Müller, M.; Nealey, P. N. *ACS Nano* **2007**, *1*, 168.

(8) Crossland, E. J. W.; Cunha, P.; Scroggins, S.; Moratti, S.; Yurchenko, O.; Steiner, U.; Hillmyer, M. A.; Ludwigs, S. *ACS Nano* **2010**, *4*, 962.

(9) Morkved, T. L.; Lu, M.; Urbas, A. M. *Science* **1996**, *273*, 931.

(10) Edwards, E. W.; Muller, M.; Stoykovich, M. P.; Solak, H. H.; de Pablo, J. J.; Nealey, P. F. *Macromolecules* **2007**, *40*, 90.

(11) Kim, S. H.; Misner, M. J.; Xu, T.; Kimura, M.; Russell, T. P. *Adv. Mater.* **2004**, *16*, 2004.

(12) Segalman, R. A.; Yokoyama, H.; Kramer, E. J. *Adv. Mater.* **2001**, *13*, 1152.

(13) (a) Baklanov, M. R.; Mogilnikov, K. P.; Polovinkin, V. G., Dultsev, F. N. 2000, *18*, 1385. (b) Baklanov, M. R.; Mogilnikov, K. P. *Microelectron. Eng.* **2002**, *64*, 335.

(14) Boissiere, C.; Grosso, D.; Lepoutre, S.; Nicole, L.; Bruneau, A. B.; Sanchez, C. *Langmuir* **2005**, *21*, 12362.

(15) (a) Jousseaume, V.; Rolland, G.; Babonneau, D.; Simon, J. P. *Thin Solid Film* **2009**, *517*, 4413. (b) Lepoutre, S.; Julian-Lopez, B.; Sanchez, C.; Amenitsch, H.; Linden, M.; Grosso, D. *J. Mater. Chem.* **2010**, *20*, 537.

(16) Faustini, M.; Vayer, M.; Marmiroli, B.; Hillmyer, M.; Amenitsch, H.; Sinturel, C.; Grosso, D. *Chem. Mater.* **2010**, *22*, 5687.

(17) Vayer, M.; Hillmyer, M. A.; Dirany, M.; Thevenin, G.; Erre, R.; Sinturel., C. *Thin Solid Film* **2010**, *518*, 3710.

(18) Zalusky, A. S.; Olayo-Valles, R.; Taylor, C. J.; Hillmyer, M. A. *J. Am. Chem. Soc.* **2001**, *123*, 1519.

(19) Paredes, J. I.; Martinez-Alonso, A.; Tascon, J. M. D. *Microporous Mesoporous Mater.* **2003**, *65*, 93.

(20) (a) Haddad, E.; Nossov, A.; Guenneau, F.; Nader, M.; Grosso, D.; Sanchez, C.; Gedeon, A. *Stud. Surf. Sci. Catal.* **2004**, *154*, 1464. (b) Kuemmel, K.; Grosso, D.; Boissière, C.; Smarsly, B.; Brezesinski, T.; Albouy, P. A.; Amenitsch, H.; Sanchez, C. *Angew. Chem., Int. Ed.* **2005**, *44*, 4589. (c) Prouzet, E.; Boissière, C.; Kim, S. S.; Pinnavaia, T. J. *Microporous Mesoporous Mater.* **2009**, *119*, 9.

(21) Tsuru, T.; Hino, T.; Yoshioka, T.; Asaeda, M. *J. Membr. Sci.* **2001**, *186*, 257.